Journal of Science and Technology in Civil Engineering, HUCE (NUCE), 2022, 16 (1): 19–28

EXPERIMENTAL INVESTIGATION OF THE SECONDARY CREEP OF FIBER REINFORCED CONCRETE AT HIGH STRESS: MACROSCOPIC MEASUREMENT AND DIGITAL IMAGE CORRELATION

Pham Duc Tho[a,*], Tran Manh Tien[b], Dang Trung Thanh[a], Vu Minh Ngan[a],

Vu Minh Ngoc[c], Luca Sorelli[d]

[a]*Faculty of Civil Engineering, Hanoi University of Mining and Geology, 18 Vien street, Bac Tu Liem district, Hanoi, Vietnam*
[b]*Department of Mechanisms of Materials, Hanoi University of Mining and Geology, 18 Vien street, Bac Tu Liem district, Hanoi, Vietnam*
[c]*Institute of Research and Development, Duy Tan University, 254 Nguyen Van Linh street, Thanh Khe district, Da Nang, Vietnam*
[d]*Department of Civil Engineering, University Laval, Pavillon Adrien-Pouliot, 1065, av. de la Médecine, Québec, G1V 0A6, Canada*

Article history:
Received 03/6/2021, Revised 24/8/2021, Accepted 31/8/2021

Abstract

The secondary creep of Fiber-Reinforced Concrete (FRC) under high sustained stress levels is a key issue for structural durability when considering the capacity to guarantee small crack widths under serviceability states. This study investigates the time-dependent deformation of FRC beams under loading level P_s/P_0 greater than 80% (P_s is the load at reloading and P_0 is the load before unloading) with various aggregate sizes by using both the classical macroscopic measurement and the digital image correlation analysis (DIC). Notched beams made of FRC and Fiber Reinforced Mortar (FRM) (i.e. without aggregate) were firstly pre-cracked by static load and then applied by a loading equal to 80% of strength. The evolution of the deflection, the crack width, and the crack propagation were both measured by traditional sensors and calculated by DIC. Comparison between results from FRC and FRM materials highlights the influence of microstructure heterogeneity on the secondary creep of FRC. Moreover, the DIC analysis helps to get insights on the secondary creep mechanism.

Keywords: fiber reinforced concrete; secondary concrete creep; damage; digital image correlation.

https://doi.org/10.31814/stce.huce(nuce)2022-16(1)-02

1. Introduction

In civil engineering, the durability of concrete structures depends significantly on time-dependent damage mechanisms induced by external loadings, aggressive environment, or other durability issues (e.g., internal expansion of reactive aggregates), which can often accelerate the creep deformation up to collapse. Excessive creep deformations of cement-based composites might cause an loss of pre-stress action of a structure and induce the structure instability [1]. Moreover, creep and damage can

*Corresponding author. *E-mail address:* phamductho@humg.edu.vn (Tho, P. D.)

be strongly coupled. Indeed, crack growth due to secondary creep creates the pathway for aggressive agents to penetrate within the concrete and to further extend damage and secondary creep. Thus, deteriorated concrete structures with reduced concrete strength and stiffness can undergo excessive creep deformation, which makes decrease the safety coefficient against failure.

In the last decades, Fiber Reinforced Concretes (FRC) have been widely used employed as an efficient in order to control the crack width and to enhance the durability of concrete structures [2–8]. Recently, the secondary creep of FRC beams under high sustained loading has also been investigated with special attention on the crack opening growth over time [9–13]. In those studies, the monitoring of the creep deformation has been usually performed via the macroscopic measurement (i.e. classical measurement with sensors). For instance, Zerbino et al. [10] performed a flexural test in four points on FRC beams having a notch at mi-span with different pre-cracking from 0.1 mm to 3.54 mm. These beams were reloaded to a force corresponding to a certain percentage of with sustained loading pre-cracking load P_s/P_0 (45% to 156%). The results showed that secondary creep of FRC beams can cause a stable crack opening rate of about 0.20 μm/h/MPa during the first month of sustained loading. The macroscopic measurement can not help to understand the mechanism of creep, as well as the coupling between damage and non-linear creep strain. Based on the correlation between the measured creep deformation and the acoustic measurement during a tensile creep test on plain concrete subjected to a high stress (with loading level in between 54% and 80%), Rossi et al. [14] assumed that the creep (at high stress level) was mainly due to an interactive process between micro-cracking and drying shrinkage. Digital Image Correlation (DIC) technique has been developed to analyse the local strain field of a material under loading. This technique can be a good candidate to study the creep strain of a specimen under loading, which is the main motivation of this study. Moreover, the effect of the aggregate heterogeneity on the creep strain has not been studied in the literature.

While the mechanisms associated to concrete creep are still not well known [15], there is a general agreement on the role of microcracking on the non-linear creep in both secondary and tertiary phases [16]. Bažant et Xiang [17] proposed a relationship between creep non linearity and micro-cracks by defining crack growth as a function of the stress intensity factor, which in turns depends on the stress level. Other mathematical models have extended linear viscoelastic models by multiplying the creep compliance by a non-linear function of the stress-state [18, 19]. Recently, models introducing the coupling between creep and damage have been developed by incorporating a stress reduction based on the damage variable associated with the creep strain [16, 20].

The aim of this study focuses on the investigation of the secondary creep of FRC under high sustained flexural loads by using both the sensors measurement and the DIC. The effect of aggregate distribution and size on the damage and secondary creep are also studied. To do so, four-point flexure testing on beams, made of FRC and FRM, are considered. The notched beam was firstly pre-cracked by a static load, then unloaded and finally applied to a sustained load to following the creep strain. The classical measurement provides the evolution in crack opening and in deflection as a function of time, while the displacement and deformation field was measured and determined by Digital Images Correlation techniques (DIC) [21, 22]. DIC technique also allow visualize the microcrack process zone around the main crack, allowing to explain the role of the development of microcracks on the secondary creep. Moreover, the effect of the aggregate heterogeneity is highlighted by the comparison between the measurement from samples made of FRC and FRM.

2. Methodology and experimental

2.1. Materials and characterization

Two materials are considered, namely FRC-05 for fiber reinforced concrete with $w/c = 0.5$ and FRM-05 for fiber reinforced mortar with $w/c = 0.5$. The mix-design for FRC-05 is presented in Table 1. The fiber reinforcement consists of hooked-end steel fibers with 30 mm length and 0.38 mm diameter (Dramix 3D80[30/0.38]. The particle size distribution of the aggregate and sand used for FRC-0.5 mixture is shown in Fig. 1. The cement is a Cement GU-SF which consists of 10% silica fume. As for curing, samples were unmolded after 24 hours and cured for 28 days in a fog chamber at 100% relative humidity (h_r). Table 2 reports the material characterization at 28 days for all both FRC-05 and FRM-05, including the mean value and the standard deviation of Young's modulus E and compressive strength f_c, which were determined from 3 repetitions. These mechanical properties were measured from the compression tests and static modulus [23] of elasticity tests [24] on the cylindrical sample with the dimension 100×200 mm^2.

Table 1. Mix-designs for the FRC materials studied in this work

Material ID	FRC-05
w/c	0.5
Cement GU-SF [kg/m^3]	550
Sand (0-2.5 mm) [kg/m^3]	801
Gravel (2.5-10 mm) [kg/m^3]	668
Steel fibres (Dramix 3D80 [30/0.38]) [kg/m^3]	78
Water [kg/m^3]	275

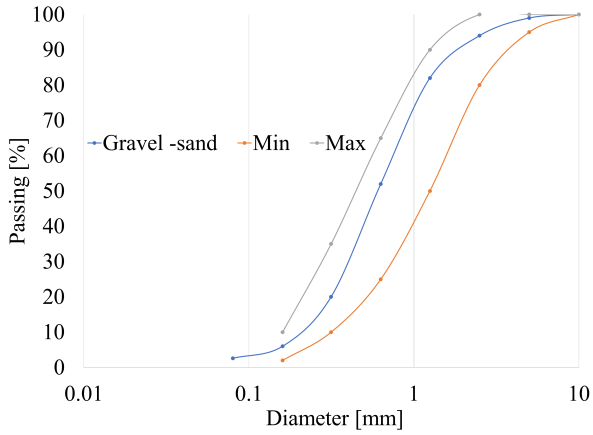

Figure 1. Granulometric curve for gravel and sand of FRC

Table 2. Material characterization at 28 days

Material ID	Young's modulus E [GPa]	Compressive strength f_c [MPa]
FRC-05	30.6±1.1	51.9±1.4
FRM-05	28.2±2.0	46.5±1.0

2.2. *Flexural creep specimens*

The beam dimensions for flexural creep tests are 100 x 40 x 400 mm^3. Each beam was notched in order to ensure the localization of a single macro-crack. After 28 days, the notches were carefully sawn at mid-span from a single blade stroke using a circular saw and measured approximately 16.0 mm deep and 4.1 mm wide. After being cured for 28 days in a fog chamber at relative humidity (R_h) 100%, all specimens were further cured in the air for at least three months in a controlled environment room at R_h = 50 ± 5% and 23 ± 2 ºC before the experimental tests.

2.3. *Test setting for flexural creep*

Following previous work [11], the creep flexural tests were carried out in three phases: (i) the beam was initially loaded by displacement control with a rate of 0.2 mm/min until the crack opening reached the initial crack opening, w_0 = 0.2 mm), the pre-cracking test is presented in Fig. 2(a). The crack openings were measured by an LVDT positioned on the side of the notch. The load corresponding to an average crack mouth opening displacement (CMOD), w_0, was called P_0 and will be used as a reference value to determine the sustained load level applied in the flexural creep test; (ii) the specimen was completely unloaded; (iii) they were reloaded and subjected to sustained load level (P_s) (Fig. 2(b)).

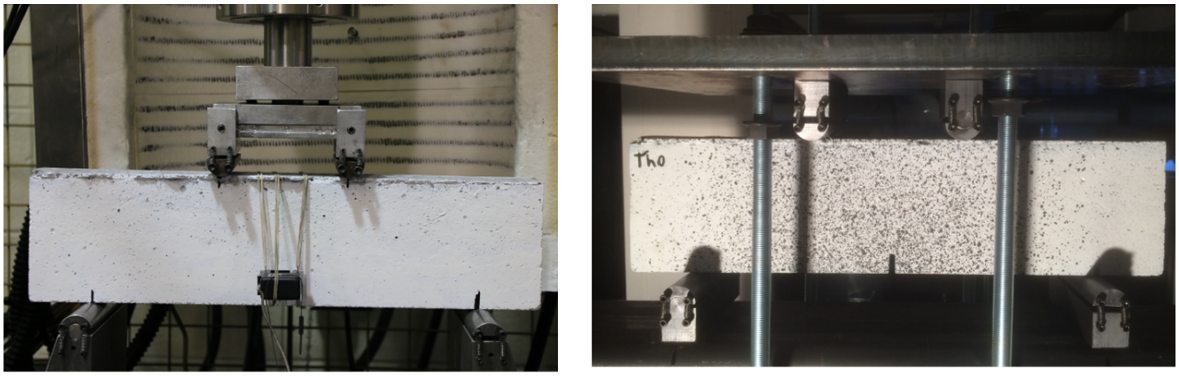

(a) Static test for pre-cracking

(b) Sustained loading test setup

Figure 2. Test set-up for the pre-cracking and flexural creep

As for the 3rd stage, a steel frame apparatus was built to load the samples with dead weight utilizing lever arms as shown in Fig. 3(b). The loading history is illustrated in Fig. 3(a).

Table 3 reports the mix-design applied in this study with the selected test setting as: the creep behavior of FRC-05 and FRM-05 was tested at 80% of maximum flexural loading capacity. All the samples were tested in a room with RH humidity of about 50% ± 5% and three test repetitions were carried out.

Table 3. Samples series and test conditions

Material ID	Load level	Relative humidity at testing	Test repeatability
FRC-05	P_s/P_0 = 80%	50% ± 5%	3
FRM-05	P_s/P_0 = 80%	50% ± 5%	3

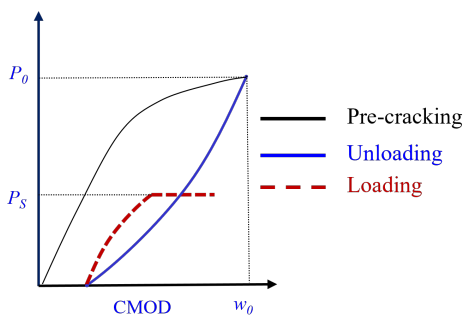

(a) Typical crack opening curve for the bending test

(b) Test set-up for the creep tests with dead weight and steel lever arms

Figure 3. Test set-up for the loading and DIC

2.4. Principe of Digital Image Correlation (DIC)

Digital image correlation was proposed at the beginning of the 1980s when applying in solid mechanics. The displacements are expressed in terms of pixels, the only quantity at hand when pictures are analyzed (Fig. 4). Let's consider $u(x)$ as displacement between the reference $f(x)$ and the deformed state $g(x)$ pictures of a surface (represented here as a grey level valued function of the pixel coordinates). The passive advection of the texture $f(x)$ by the displacement field creates a "deformed image," $g(x)$ [21, 22]:

$$g(x)=f(x+u(x)) \tag{1}$$

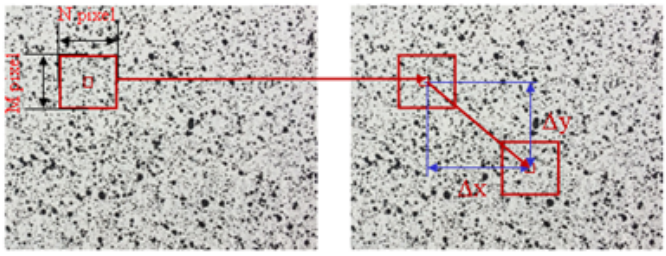

Figure 4. The initial and deformed image

Eq. (1) is the conservation of the "optical flow" The problem to address is the determination of the displacement field $u(x)$ from the exclusive knowledge of $f(x)$ and $g(x)$. Eq. (1) is linearized by assuming that the reference image is differentiable.

$$\phi^2(x) = [u(x).\nabla f(x) + f(x) - g(x)]^2 \tag{2}$$

To estimate $u(x)$ it needs to minimize the quadratic difference over the studied domain Ω:

$$\eta^2(x) = \int_{\Omega} [u(x).\nabla f(x) + f(x) - g(x)]^2 dx \tag{3}$$

For measuring the deflection and crack opening, the initial picture is taken as a reference position. The beam zone investigated by DIC (with an element size of 24 pixels) in this work is shown in

Fig. 5(a). As an example of case FRC-05, Fig. 6(b) and Fig. 6(c) show the displacement field in the x and y directions. The colour discontinuity shows the crack pattern obtained after loading. The crack opening was measured by the difference of axial displacement (x-direction) of two points at the notched while the deflection was obtained from the displacement field (y-direction). Furthermore, the error map allows observing the micro-crack. The micro-crack surrounding the macro-crack is observed, which is due to the new crack that appeared. The example in Fig. 6 shows also the effect of aggregate to slightly deviate the crack trajectory.

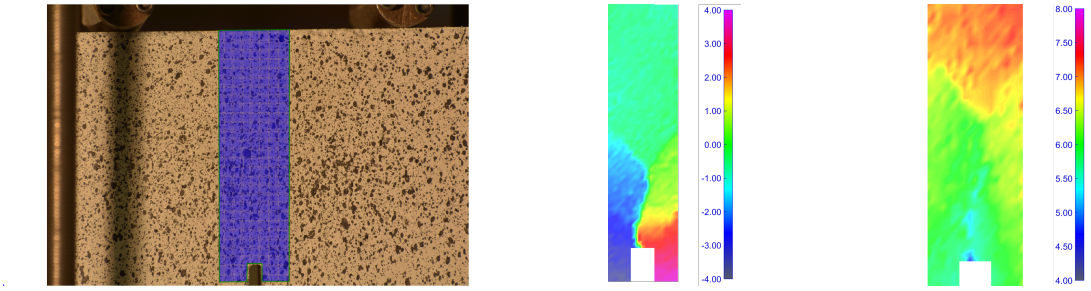

(a) Window analyzed by DIC astride the beam notch (b) Horizontal displacement map in pixels (c) Vertical displacement map in pixels (b) (1 pixel = 28.5 µm)

Figure 5. The beam zone investigated by DIC

Finally, the effect of the mesh is shown in Fig. 6 for the elements with sizes 16 and 24 pixels. As observed, the element size has a negligible influence on the measured results.

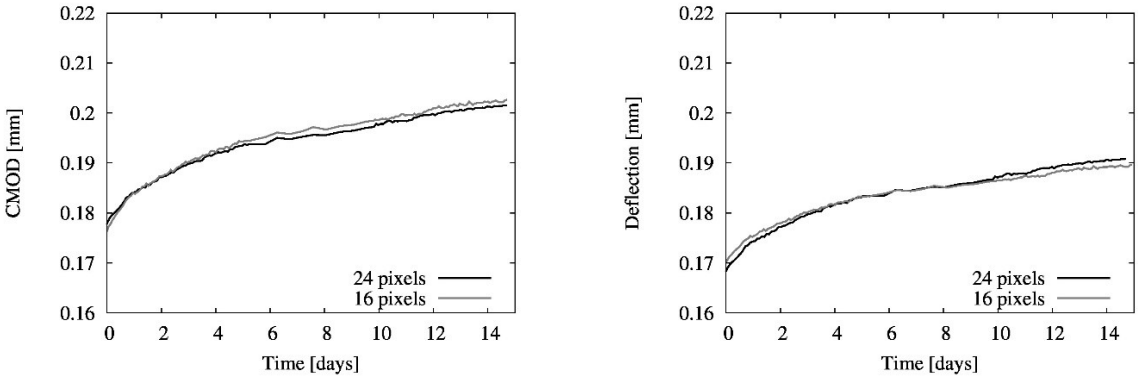

(a) CMOD - Time (b) Deflection - Time

Figure 6. Comparison of displacement jump profiles for different element sizes

3. Results and discussion

3.1. Static tests

Fig. 7 shows the results of the static tests for pre-cracking the beams made of FRC-05 and FRM-05. The mean flexural load-bearing capacity are of about 9 kN and 7 kN for FRC-05 and FRM-05

beams, respectively. As shown in Fig. 3(a), the pre-cracking phase successfully damages the sample with an initial crack width of about 100 μm for all FRC and FRM samples.

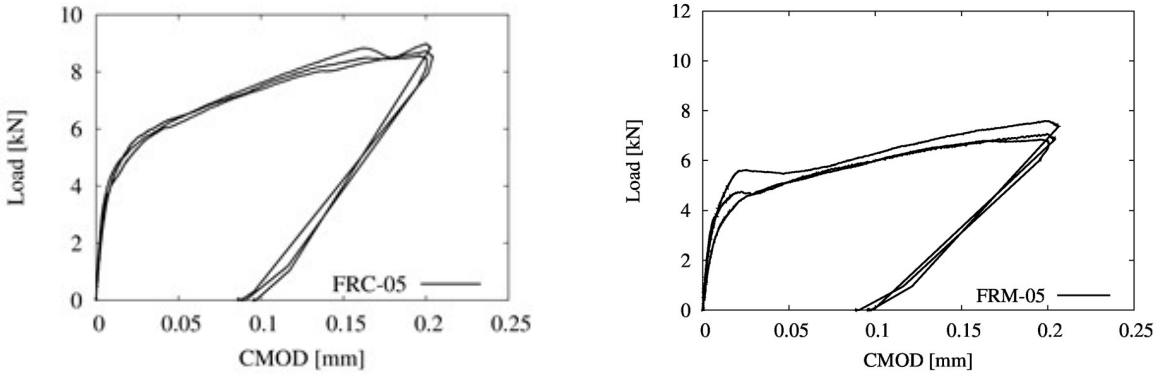

(a) FRC-05 (b) FRM-05

Figure 7. Crack opening-load responses

3.2. Creep tests

The main results of the creep tests are shown in Fig. 8 in terms of crack opening (CMOD) versus time and deflection versus time for FRC-05 beams. The figures are zoomed on the curves to emphasize the differences. The test repeatability was rather satisfactory. After a primary creep phase in 3-4 days, all the FRC exhibited a secondary creep phase, which is rather linear with time, but the test duration was not enough to observe the tertiary creep.

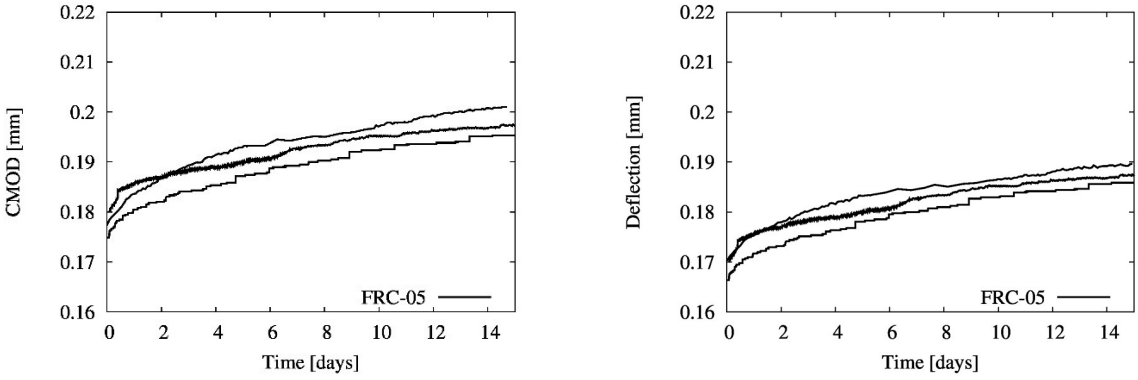

(a) CMOD and time (b) Deflection and time

Figure 8. Creep response of FRC-05

a. Effect of aggregate heterogeneity

Fig. 9 compares the mean curves of FRC-05 and FRM-05 (absence of aggregate) in terms of CMOD versus time and deflection versus time, respectively. The comparison shows the effect of aggregate on the creep response. As observed, the aggregate heterogeneity increases the secondary

creep in terms of CMOD rate. The deflection comparison is less evident due to the initial elastic deformation of FRM that was slightly higher. However, if the deflection rate achieved at 14 days is considered, the aggregate heterogeneity of FRC-05 showed a larger slope.

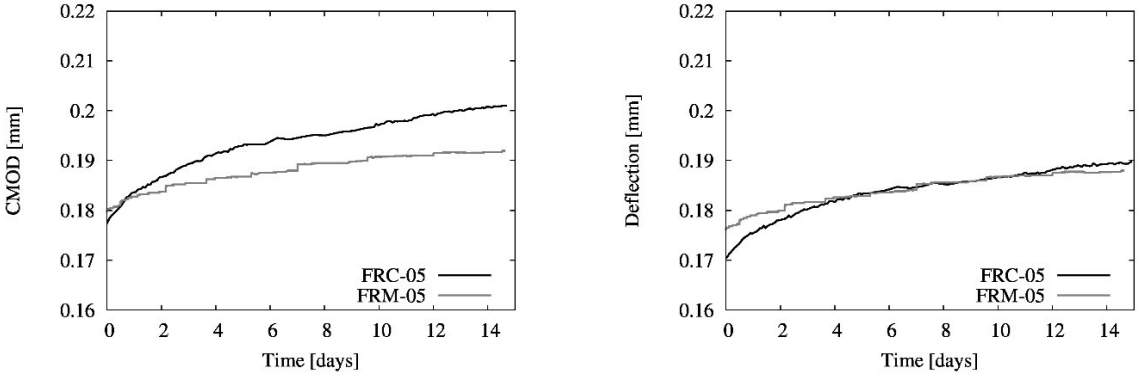

(a) CMOD and time

(b) Deflection and time

Figure 9. Effect of aggregate heterogeneity

b. DIC crack detection

DIC analysis is finally carried out to observe the crack growth and the presence of microcracks. Fig. 10 illustrates the macro-crack of the creep tests for a FRC-05 specimen. It is also possible to observe a microcracking process zone around the major crack at the end of creep tests. These results confirm that at high sustained loadings, the secondary creep is mainly due to the crack propagation with a developed microcracking process zone. These conclusions confirm the hypothesis proposed by Rossi et al. [14], assuming that the creep of concrete (at high stress) was mainly due to microcracking and its kinetics depends on the presence of the water movement.

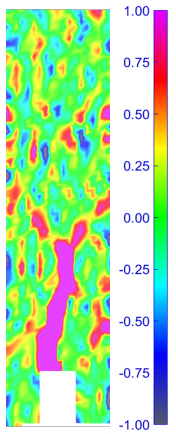

Figure 10. Deformation ε_{xx} (%) FRC-05

4. Conclusions

In this study, an experimental investigation was carried out to characterize the secondary creep of pre-cracked FRC beams under flexural high sustained loading. The effect of aggregate heterogeneity is considered by comparing the measurement from both FRC and FRM beams. Based on good repeatability of the present results, the following main conclusion can be drawn:

- The effect of aggregate size was also found to be a significant factor on the secondary creep rate of FRC. By comparing a fiber reinforced concrete and mortar with a similar amount of cement paste, increasing the aggregate size from 2.5 mm to 10 mm enhanced the crack width rate of about 30%;

- The DIC analysis confirmed the importance of the crack growth and microcrack process zone on the secondary creep.

The study results are the database for modeling non-linear creep with respect to material parameters and testing conditions allows for a bidirectional analysis in terms of plain stress and hygral distribution. Future works are needed to disclose the effect of the material parameters on the time of the collapse, (e.g. extending the duration time to several dozen days) and the effect of external relative humidity of the external environment on the secondary creep. The behavior of secondary creep of normal concrete without fibers also deserves to be investigated.

References

[1] Bažant, Z., Li, G. H., Yu, Q., Klein, G., Kristek, V. (2008). Explanation of Excessive Long-Time Deflections of Collapsed Record-Span Box Girder Bridge in Palau, Preliminary report. In *The 8th International Conference on Creep and Shrinkage of Concrete*, volume 30, 1–31.

[2] Banthia, N. (1994). Fiber reinforced concrete. *ACI SP-142ACI Detroit MI*, 91–119.

[3] Hilsdorf, H., Kropp, J. (2004). *Performance criteria for concrete durability*, volume 12. CRC Press.

[4] Mehta, P. K. (1991). Durability of concrete–fifty years of progress? *ACI Special Publication*, 126:1–32.

[5] Mehta, P. K. (1986). *Concrete. Structure, properties and materials*.

[6] Bui, T. S., Pham, D. T., Vu, M. N., Nguyen, T. N., Nguyen-Sy, T., Nguyen, V. P., Nguyen-Thoi, T. (2021). Modeling of the tension stiffening behavior and the water permeability change of steel bar reinforcing concrete using mesoscopic and macroscopic hydro-mechanical lattice model. *Construction and Building Materials*, 291:123266.

[7] Pham, D. T., Sorelli, L., Fafard, M., Vu, M.-N. (2020). Hydromechanical couplings of reinforced tensioned members of steel fiber reinforced concrete by dual lattice model. *International Journal for Numerical and Analytical Methods in Geomechanics*, 45(2):191–207.

[8] Tien, T. M., Vu, X. H., Ferrier, E., Tho, P. D., Loan, B. T. (2021). Experimental investigation and analytical modeling of the crack width effect on the fire performance of carbon textile-reinforced concrete composite. *Journal of Science and Technology in Civil Engineering (STCE)-HUCE*, 15(3):81–92.

[9] Abrishambaf, A., Barros, J. A., Cunha, V. M. (2015). Time-dependent flexural behaviour of cracked steel fibre reinforced self-compacting concrete panels. *Cement and Concrete Research*, 72:21–36.

[10] Zerbino, R. L., Barragan, B. E. (2012). Long-Term Behavior of Cracked Steel Fiber-Reinforced Concrete Beams under Sustained Loading. *ACI Materials Journal*, 109(2):215–224.

[11] Daviau-Desnoyers, D., Charron, J.-P., Massicotte, B., Rossi, P., Tailhan, J.-L. (2015). Characterization of macrocrack propagation under sustained loading in steel fibre reinforced concrete. *Materials and Structures*, 49(3):969–982.

[12] Rossi, P., Boulay, C., Tailhan, J.-L., Martin, E., Desnoyers, D. (2014). Macrocrack propagation in concrete specimens under sustained loading: Study of the physical mechanisms. *Cement and Concrete Research*, 63:98–104.

[13] García-Taengua, E., Arango, S., Martí-Vargas, J., Serna, P. (2014). Flexural creep of steel fiber reinforced concrete in the cracked state. *Construction and Building Materials*, 65:321–329.

[14] Rossi, P., Tailhan, J.-L., Maou, F. L., Gaillet, L., Martin, E. (2012). Basic creep behavior of concretes investigation of the physical mechanisms by using acoustic emission. *Cement and Concrete Research*, 42 (1):61–73.

[15] Xi, Y.-P., Jennings, H. M. (1992). Relationships between microstructure and creep and shrinkage of cement paste. *Mater. Sci. Concr., IIIpp.*, 37.

[16] Mazzotti, C., Savoia, M. (2003). Nonlinear Creep Damage Model for Concrete under Uniaxial Compression. *Journal of Engineering Mechanics*, 129(9):1065–1075.

[17] Bažant, Z. P., Xiang, Y. (1997). Crack Growth and Lifetime of Concrete under Long Time Loading. *Journal of Engineering Mechanics*, 123(4):350–358.

[18] Bažant, Z. P., Prasannan, S. (1989). Solidification Theory for Concrete Creep. I: Formulation. *Journal of Engineering Mechanics*, 115(8):1691–1703.

[19] Ruiz, M. F., Muttoni, A., Gambarova, P. G. (2007). Relationship between Nonlinear Creep and Cracking of Concrete under Uniaxial Compression. *Journal of Advanced Concrete Technology*, 5(3):383–393.

[20] Reviron, N., Benboudjema, F., Torrenti, J. M., Nahas, G., Millard, A. (2007). Coupling between creep and cracking in tension. In *6th International Conference on Fracture Mechanics of Concrete and Concrete Structures, Italie*.

[21] Réthoré, J., Hild, F., Roux, S. (2007). Shear-band capturing using a multiscale extended digital image correlation technique. *Computer Methods in Applied Mechanics and Engineering*, 196(49-52):5016–5030.

[22] Réthoré, J., Roux, S., Hild, F. (2007). From pictures to extended finite elements: extended digital image correlation (X-DIC). *Comptes Rendus Mécanique*, 335(3):131–137.

[23] CSA-A23.2-9C-09 (2009). *Compressive Strength of Cylindrical Concrete Specimens. Mississauga, Ontario, Canada, Association canadienne de normalisation*. Mississauga, Ontario, Canada.

[24] ASTM C469/C469M - 14 (2014). *Standard Test Method for Static Modulus of Elasticity and Poisson's Ratio of Concrete in Compression*. ASTM International, USA.